Large-Area, Flexible $Ti_3C_2T_x$/ $SnSe_2$ nanohybrid based Multifunctional Physical E-Textile Sensor (Pressure, Strain and Temperature) for Non-Invasive Healthcare Monitoring

*Vivek Adepu[1], Krutarth Kamath[2], Sukruth Siddhartha[1], Venkat Mattela[3], and Parikshit Sahatiya[1]**

[1] *Department of Electrical and Electronics Engineering, Birla Institute of Technology and Science Pilani Hyderabad Campus, Hyderabad, 500078, India.*

[2]*Department of Chemical Engineering, Birla Institute of Technology and Science Pilani Hyderabad Campus, Hyderabad, 500078, India.*

[3]*Ceremorphic, Inc. San Jose, California, 95131, USA*

**E-mail of Corresponding Author: parikshit@hyderabad.bits-pilani.ac.in.*

Abstract:

Herein, we fabricated $Ti_3C_2T_x$/ $SnSe_2$ nanohybrid based multifunctional physical sensors (pressure, strain, and temperature) on the cotton substrate for non-invasive healthcare monitoring. The fabricated nanohybrid E-textile based physical sensors displayed an improved sensitivity of 14.959 kPa^{-1} for 1.477 – 3.456 kPa of the applied external pressure and an enhanced gauge factor of 14.108 for 5-25% of applied strain. In addition, these physical sensors have shown exceptional stability

of ~2500 cycles for a pressure sensor and ~3000 cycles for a strain sensor which signifies the sturdiness of the sensor. Furthermore, the fabricated temperature sensor has displayed a TCR value of 7.943 x 10^{-3} $^{o}C^{-1}$ and a high activation energy value of 300.684 meV. Further, an android/iOS/web-based app was developed to validate wireless integration of the fabricated multifunctional physical sensors by utilizing a simple electronic circuit. Also, there are no investigations/reports on $Ti_3C_2T_x$/ $SnSe_2$ nanohybrid physical sensor-based applications as per the author's knowledge. The successful demonstration of $Ti_3C_2T_x$/ $SnSe_2$ nanohybrid E-textile based multifunctional physical sensor commences new possibilities for advanced health care and medical applications.

Keywords: $Ti_3C_2T_x$/ $SnSe_2$ nanohybrid, multifunctional sensor, non-invasive, TCR, activation energy.

Introduction:

Recently, leading a sedentary lifestyle has become a severe public health issue, with many inactive individuals prone to various health risks, including depression and anxiety, obesity, diabetes, and even cardiovascular diseases. Moreover, in a recent survey, physical inactivity was ranked as the fourth most significant risk for deaths in the world. To monitor the physical activity and quantify the plantar pressure, we can use the conventional method, which is inexpensive but can produce an error while reporting physical activity. Further, we can also use other techniques pedometers, heart rate monitors etc., which extensively depends on the number and type of sensors used to monitor various physical movements such as walking, running etc. A wearable smart shoe integrated with inexpensive and flexible sensors seems like a possible solution for the inconspicuous monitoring of human activities precisely is an urgent prerequisite in this context.

In the recent past, E-textiles based physical sensors were found as probable candidates for issues mentioned above owing to intriguing properties such as ultra-lightweight, conformable to the skin, air permeability, flexibility, stretchability etc., Further, due to these inherent properties, E-textiles were considered as perfect substrates for flexible and wearable electronics. Moreover, smart textiles are also used in a wide range of real-time applications, such as human-machine interaction to monitor various human motions, artificial e-skin, electromagnetic interface shielding etc. E-textile-based physical sensors have several configurations such as piezoresistive type, capacitive type, piezoelectric. In particular, the piezoresistive type physical sensors have attained immense interest owing to simplistic and inexpensive device fabrication, improved sensitivity and solidity and ease of data procurement in the broad sensing range.

The active material on the flexible E-textile substrate based physical sensor plays a crucial role in its performance. Several nanomaterials such as 0D, 1D, 2D and 3D nanomaterials families were potential active materials for E-textiles. Explicitly, 2D nanomaterials such as graphene, borophene, black phosphorus, TMD's (transition metal dichalcogenides), covalent organic frameworks, MXenes (Metal carbides/nitrides), etc., are an excellent choice as active material owing to the high specific surface area, improved electrical, physical, and mechanical properties etc. for piezoresistive based physical sensors. MXenes with $M_{n+1}X_nT_x$ formula have displayed potential applications for physical and chemical sensors, energy generation and storage, advanced healthcare systems etc. Specifically, titanium carbide ($Ti_3C_2T_x$) MXene with a nanolayered accordion-like structure has achieved an enormous amount of consideration due to its captivating properties, such as extraordinary electrical conductivity comparable to that of graphene, highly hydrophilic, tunable surface chemistry due to the presence of diverse functional groups in the chemical structure etc. Additionally, the bandgap and work function of MXenes can be restrained

by tailoring its structure and functional groups. Moreover, TMD's, a well-explored family of 2D nanomaterials, has been widely used for sensors due to their remarkable properties, such as layered atomic structure, etc. Recently, it was noticed that there are very few reports for MXene/TMD's based composites and further have a wide range of scope for their utilization in piezoresistive based physical sensors.

In the present study, we deposited $Ti_3C_2T_x$/ $SnSe_2$ thin-film on the cotton substrate *via a* cost-effective one-step hydrothermal approach followed by Dip coating technique and later fabricated multifunctional physical sensors (pressure, strain, and temperature) for non-invasive health care applications. The fabricated nanohybrid E-textile based physical sensors, i.e. pressure and strain, displayed an enhanced sensitivity of 14.959 kPa^{-1} for 1.477–3.456 kPa of the applied external pressure and an improved gauge factor of 14.108 for 5-25% of applied strain. Also, these physical sensors have shown exceptional stability of ~2500 cycles for a pressure sensor and ~3000 cycles for a strain sensor which signifies the sturdiness of the sensor. Furthermore, the fabricated temperature sensor has displayed a TCR value of 7.943 x 10^{-3} $^oC^{-1}$ and a high activation energy value of 300.684 meV. Further, an android/iOS/web-based app was developed to validate wireless integration of the fabricated multifunctional physical sensors by utilizing a simple electronic circuit. Also, there are no investigations/reports on $Ti_3C_2T_x$/ $SnSe_2$ nanohybrid physical sensor-based applications as per the author's knowledge. The successful demonstration of $Ti_3C_2T_x$/ $SnSe_2$ nanohybrid E-textile based multifunctional physical sensor commences new possibilities for advanced health care and medical applications.

Experimental Section:

Materials:

The materials tin chloride ($SnCl_2.2H_2O$), selenium (Se), sodium borohydride ($NaBH_4$), lithium fluoride (LiF), hydrochloric acid (HCl) were obtained from Sigma Aldrich, titanium aluminium carbide (Ti_3AlC_2) was procured from intelligent materials private limited, and further these materials are utilized to synthesize $SnSe_2$ *via* the hydrothermal method and MXene ($Ti_3C_2T_x$) *via* the MILD (Minimally Intensive Layer Delamination) method.

Synthesis and Device Fabrication:

Synthesis of $Ti_3C_2T_x$ solution and fabrication $Ti_3C_2T_x$ / $SnSe_2$ nanohybrid device:

The $Ti_3C_2T_x$ solution was synthesized using the MILD method reported by the group in an earlier report.[1] In brief, 800 mg of LiF powder, 500 mg of Ti_3AlC_2 powder were added to 10 ml of 6M HCl and kept for the constant stirring of 36 hrs. The resultant solution was then processed through repeated cycles of centrifugation, decantation of supernatant and dilution with DI water until the pH reached ~6-7. The solution was then subjected to probe sonication in an ice bath to attain the final $Ti_3C_2T_x$ colloidal solution.

The nutrient and seed solutions of $SnSe_2$ were prepared as follows: Initially, to prepare a nutrient solution, 90 mM of Se powder, 100 mM of $NaBH_4$ was added to 30 mL of DI water and kept for 5 minutes of stirring. Subsequently, 8.3 mM of $SnCl_2.2H_2O$ was added to the above mixture and kept for 30 minutes of incessant stirring to attain the $SnSe_2$ nutrient solution. Later, the seed solution was prepared by adding 9mM of Se powder, 10 mM of $NaBH_4$, 0.83 mM of $SnCl_2.2H_2O$ in 20 mL of DI water and keeping for 20 minutes of stirring.

Finally, the fabrication of the $Ti_3C_2T_x$ / $SnSe_2$ nanohybrid device was done in three steps. In step 1, the as-synthesized $Ti_3C_2T_x$ colloidal solution was utilized to deposit $Ti_3C_2T_x$ thin film on

the oxygen plasma activated cotton substrate by employing the dip-coating technique. In step 2, the $Ti_3C_2T_x$ deposited cotton substrate was placed in the above-prepared $SnSe_2$ seed solution for 1 hour, which generated the nucleation sites necessary to facilitate the growth of $SnSe_2$ nanostructures. Later, the substrate was transferred to a 50 mL Teflon lined stainless autoclave, which contained the $SnSe_2$ nutrient solution and was maintained for 24 hours at 180°C reaction temperature. In step 3, the resultant cotton substrate with $Ti_3C_2T_x$ / $SnSe_2$ film was encapsulated in PDMS (i.e., a two-part polymer) followed by Cu contacts formation on the substrate using Ag (silver) paste.

The entire process flow for the synthesis of $Ti_3C_2T_x$ solution, fabrication of $Ti_3C_2T_x$ / $SnSe_2$ nanohybrid sensor is illustrated in figure 1 below.

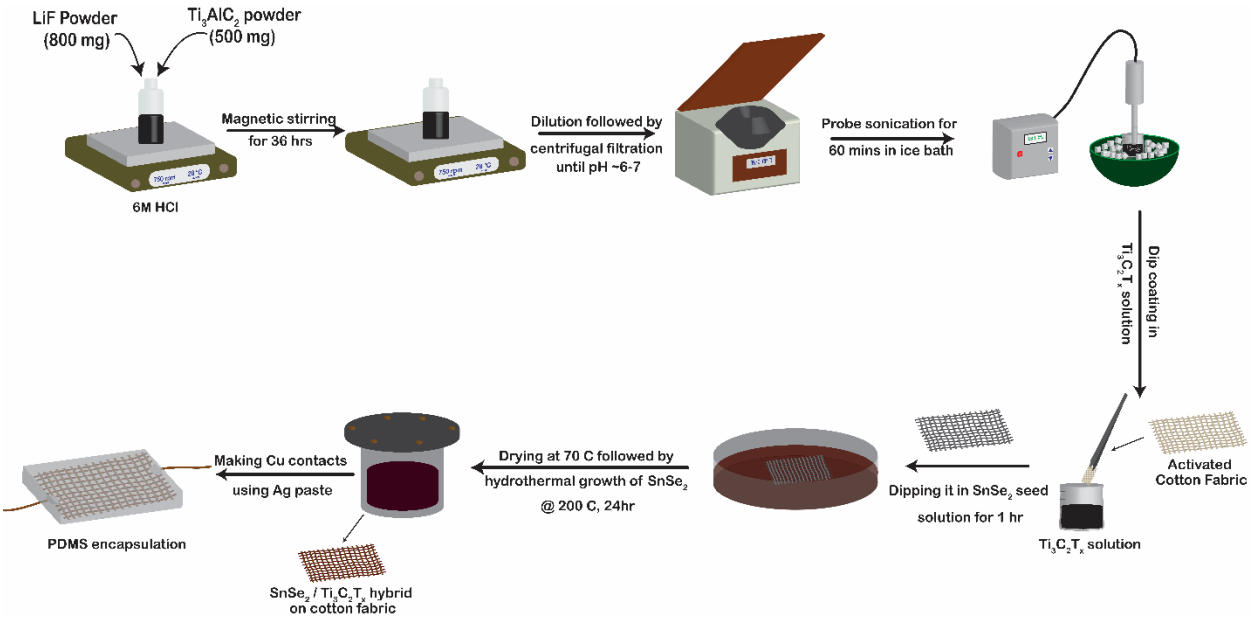

Figure 1: Schematic illustration for the synthesis of $Ti_3C_2T_x$ solution, $Ti_3C_2T_x$ / $SnSe_2$ nanohybrid sensor fabrication.

Results and Discussions:

Material Characterization:

The XRD diffraction pattern of $Ti_3C_2T_x$ / $SnSe_2$ nanohybrid thin film deposited on the cotton substrate is displayed in figure 2a below. The obtained XRD pattern confirms the existence of $SnSe_2$ with JCPDS number 89-2939 (hexagonal crystal structure) with conventional diffraction patterns with planes (0 0 1), (1 0 0), (0 1 1), (0 0 3), (1 1 1), (1 0 3) and also in particular enhanced (0 0 1) facet diffraction peak validates the [0 0 1] oriented structure of $SnSe_2$. The absence of the peak at 39^o and the shift of peak pattern from 9.5^o to 6.2^o from the XRD spectra of Ti_3AlC_2 (with JCPDS number 52-0875) justifies the formation of $Ti_3C_2T_x$ after successful elimination of Al. Figure 2b depicts the XPS survey spectra of $Ti_3C_2T_x$ / $SnSe_2$ ranging in between 0 to 800 eV. Figure 2c shows the deconvoluted XPS spectra of Ti 2p, consisting of 4 doublet peaks after core-level fitting (i.e., Ti $2p_{3/2}$, Ti $2p_{1/2}$), wherein each doublet is separated by the binding energy of 5.95 eV with an area ratio of 1:2. In particular, TiO_2 (Ti (IV)), Ti (III) (Ti_xO_y), Ti (II) (Ti-X), Ti-C (Ti (I)) are the components of Ti $2p_{3/2}$, in which Ti (II) (Ti-X) attributes to substoichiometric titanium oxycarbides/carbides.[2] The existence of TiO_2 was due to partial oxidation that occurred during the thin film deposition of $Ti_3C_2T_x$ on the cotton substrate in open atmospheric conditions. Figure 2d displays deconvoluted XPS spectra of C 1s with 5 components after fitting ascribed to -COO, C-O, $-CH_3$, $-CH_2$, C-C, Ti-C. Figure 2e depicts the deconvoluted XPS spectra of O 1s with 4 components after fitting allocated to adsorbed H_2O on the surface, Ti- OH, TiO_2, substoichiometric TiO_x, respectively. Figure 2f displays the deconvoluted XPS spectra of Sn 3d with two electronic states Sn $3d_{5/2}$ and Sn $3d_{3/2}$, wherein two electronic states are separated by 8.36 eV binding energy in the fitted spectra. Figure 2g depicts the deconvoluted XPS spectra of Se 3d with two electronic states Se $3d_{5/2}$ and Se $3d_{3/2,}$ at 54.47 and 55.54 eV B.E., and also deconvoluted

XPS spectra reveal a big shoulder peak of Ti 3s beside with Se 3d from 63 to 57 eV B.E. explicitly attributed to $Ti_3C_2F_x$/ TiO_2, Ti-C, at B.E.'s 62 eV, 60 eV respectively.[3,4] Figure 2h illustrates the Raman spectra of $Ti_3C_2T_x$ / $SnSe_2$ nanohybrid, ranging between 100 – 800 cm^{-1} Raman shift. Moreover, peak attained at 110, 180.95 cm^{-1} Raman shifts attributed to shear mode (in-plane - E_g), first-order out-of-plane (A_{1g}) vibrations, which validates the existence of the $SnSe_2$. Subsequently, peaks obtained at 204, 600 cm^{-1} Raman shifts ascribed to A_{1g} (first-order out-of-plane vibrations) and characteristic peaks obtained at 403, 630 cm^{-1} assigned to E_g (in-plane/shear mode of vibrations), which substantiates the presence of $Ti_3C_2T_x$ in Raman spectra of $Ti_3C_2T_x$ / $SnSe_2$ nanohybrid.[5,6]

Figure 3a-d illustrates the high-resolution FESEM images of $Ti_3C_2T_x$ / $SnSe_2$ thin film deposited on a cotton substrate. In detail, nanoballs-like structures of $SnSe_2$ with a typical diameter ~827 nm were grown on the layered $Ti_3C_2T_x$ deposited on the cotton substrate, which is depicted in figure 3c below in the top-view FESEM image. Also, $Ti_3C_2T_x$ / $SnSe_2$ thin-film deposited on the cotton substrate from the cross-sectional view of FESEM displayed in figure 3d.

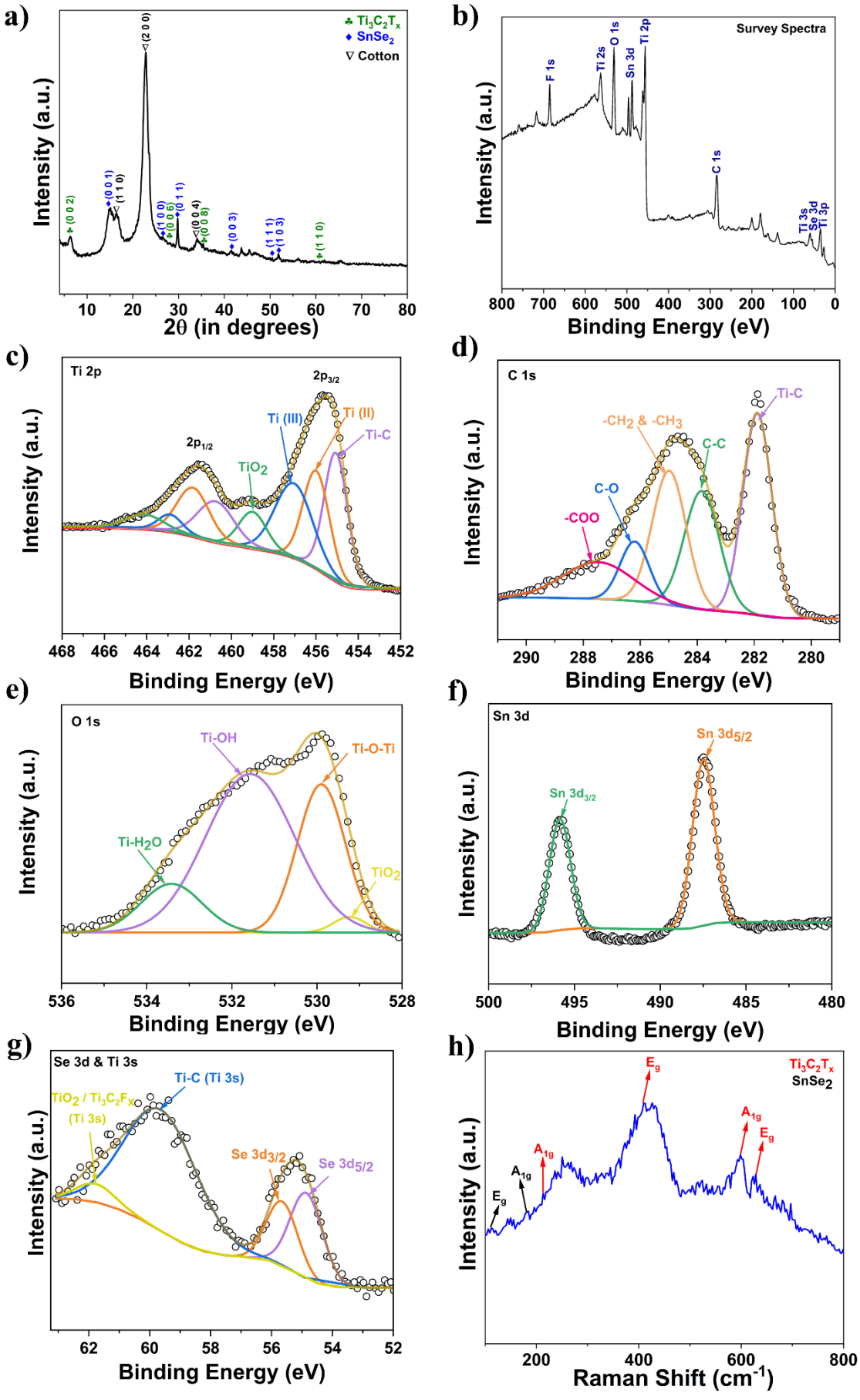
a)
♣ Ti3C2Tx
♦ SnSe2
∇ Cotton
(0 0 2)
(0 0 1)
(1 1 0)
(2 0 0)
(1 0 0)
(0 0 6)
(0 1 1)
(0 0 4)
(0 0 8)
(0 0 3)
(1 1 1)
(1 0 3)
(1 1 0)
Intensity (a.u.)
2θ (in degrees)
b)
Survey Spectra
F 1s
Ti 2s
O 1s
Sn 3d
Ti 2p
C 1s
Ti 3s
Se 3d
Ti 3p
Intensity (a.u.)
Binding Energy (eV)
c)
Ti 2p
2p3/2
2p1/2
Ti (III)
Ti (II)
Ti-C
TiO2
Intensity (a.u.)
Binding Energy (eV)
d)
C 1s
Ti-C
-CH2 & -CH3
C-C
C-O
-COO
Intensity (a.u.)
Binding Energy (eV)
e)
O 1s
Ti-OH
Ti-O-Ti
Ti-H2O
TiO2
Intensity (a.u.)
Binding Energy (eV)
f)
Sn 3d
Sn 3d5/2
Sn 3d3/2
Intensity (a.u.)
Binding Energy (eV)
g)
Se 3d & Ti 3s
Ti-C (Ti 3s)
TiO2 / Ti3C2Fx
(Ti 3s)
Se 3d3/2
Se 3d5/2
Intensity (a.u.)
Binding Energy (eV)
h)
Eg
A1g
Ti3C2Tx
SnSe2
Intensity (a.u.)
Raman Shift (cm-1)

Figure 2: a) XRD pattern of $Ti_3C_2T_x$ / $SnSe_2$ nanohybrid b) XPS Survey spectra of $Ti_3C_2T_x$ / $SnSe_2$ nanohybrid, c), d), e), f), g), h), Deconvoluted XPS spectra's of Ti 2p, C 1s, O1s, Sn 3d, Se 3d, h) Raman spectra of $Ti_3C_2T_x$ / $SnSe_2$ nanohybrid

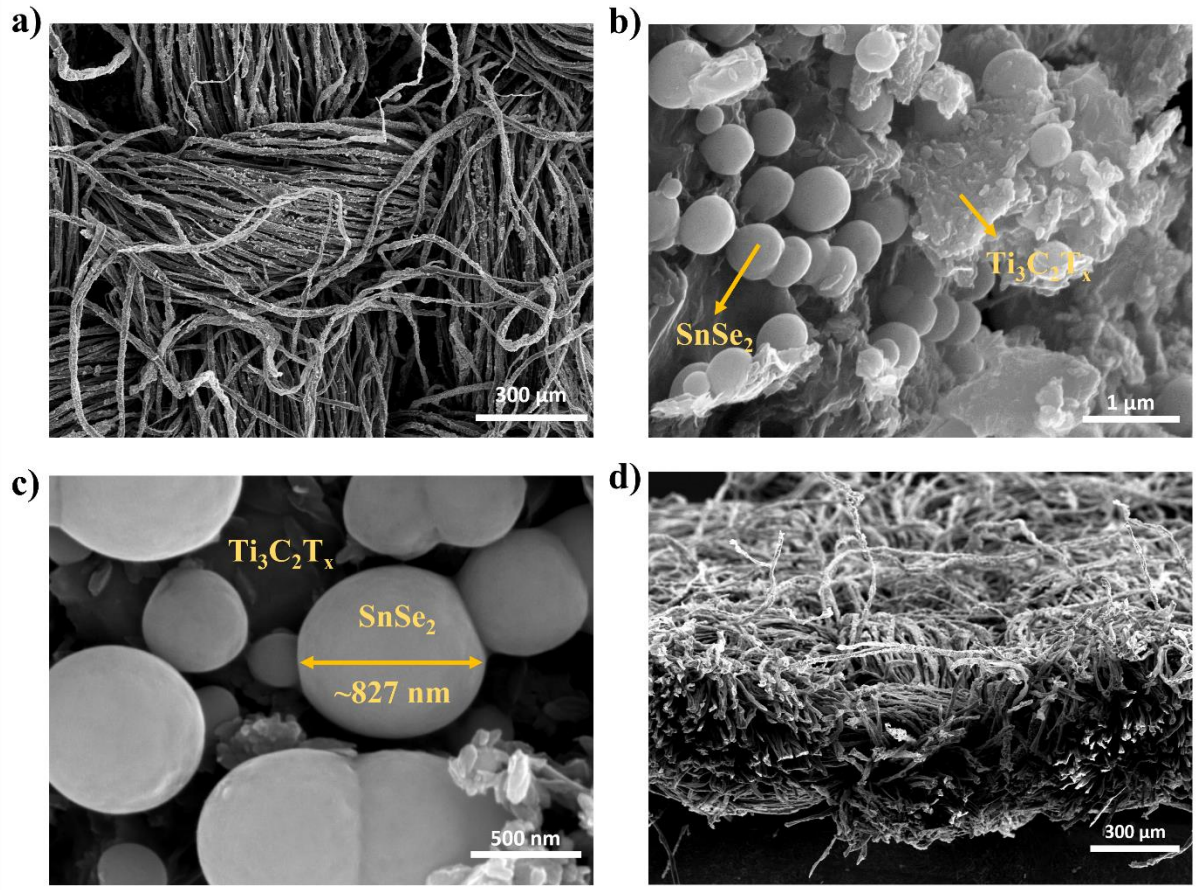

Figure 3: a), b), c) are High-resolution FESEM images of $Ti_3C_2T_x$ / $SnSe_2$ thin film deposited on the cotton in top view, d) High-resolution FESEM images of $Ti_3C_2T_x$ / $SnSe_2$ thin film deposited on the cotton in cross-sectional view

Pressure Sensing:

The fabricated $Ti_3C_2T_x$ / $SnSe_2$ nanohybrid sensor with 3 cm x 2 cm dimensions was encapsulated in PDMS was utilized for pressure characterization by applying an external bias of 1 volt. The digital image of the fabricated sensor is shown in figure 4a. Figure 4b shows the I-V characteristics

of the fabricated sensor in between -1V to 1V voltage range, which displayed the upsurge in the value of the current response with a proportionate increase in the value of the applied pressure. In figure 4c, it was noticed that the sensor was capable of detecting the applied pressure of ~2.456 kPa, which depicts the repeatability of the sensor response. The temporal response plots displayed in Figures 4d and 4e validate that the increase in the current response was attained by an increase in the external pressure applied which was found unfailing with the I-V characteristics of the fabricated sensor. The sensitivity of the fabricated sensor displayed in figure 4f below was exceptional, with a value of 14.959 kPa^{-1} compared to the existing state of the art for MXene/TMD's nanohybrid based pressure sensors explained in table 1. In addition, in pressure sensing performance, figure 4g depicts the sturdiness of the fabricated sensor, which endures ~2500 cycles without a conspicuous change in the current response. Finally, figure 4h signifies the response and recovery time of the sensor as ~99 msec and ~187 msec, respectively.

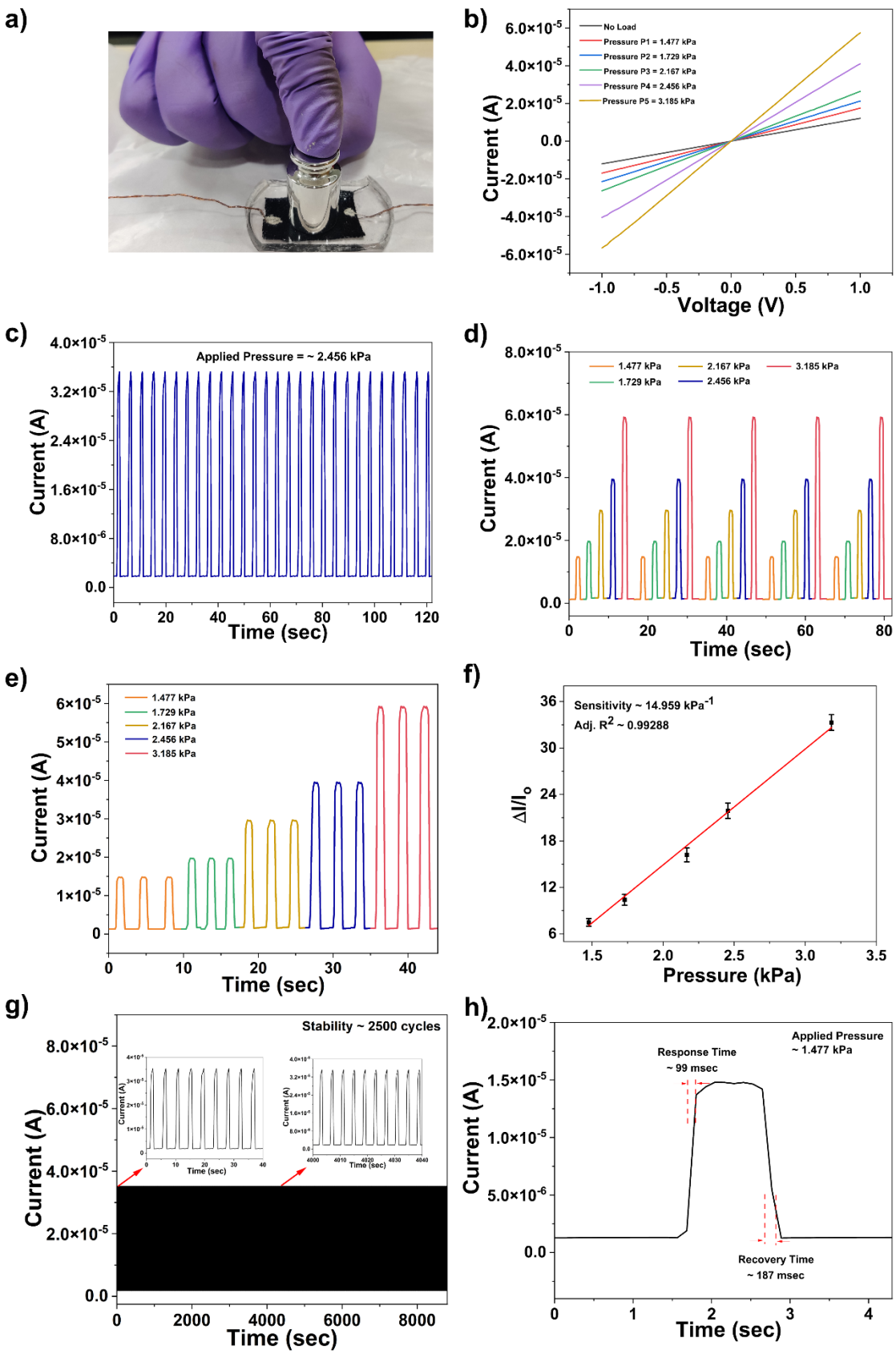
a)
b)
No Load
Pressure P1 = 1.477 kPa
Pressure P2 = 1.729 kPa
Pressure P3 = 2.167 kPa
Pressure P4 = 2.456 kPa
Pressure P5 = 3.185 kPa
Current (A)
Voltage (V)
c)
Applied Pressure = ~ 2.456 kPa
Current (A)
Time (sec)
d)
1.477 kPa
1.729 kPa
2.167 kPa
2.456 kPa
3.185 kPa
Current (A)
Time (sec)
e)
1.477 kPa
1.729 kPa
2.167 kPa
2.456 kPa
3.185 kPa
Current (A)
Time (sec)
f)
Sensitivity ~ 14.959 kPa-1
Adj. R2 ~ 0.99288
ΔI/Io
Pressure (kPa)
g)
Stability ~ 2500 cycles
Current (A)
Time (sec)
h)
Applied Pressure
~ 1.477 kPa
Response Time
~ 99 msec
Recovery Time
~ 187 msec
Current (A)
Time (sec)

Figure 4: Pressure characterization of $Ti_3C_2T_x$ / $SnSe_2$ nanohybrid sensor a) Digital image of the fabricated sensor with weight loaded on to it, b) I-V characteristics of the fabricated sensor, c),d),e) Temporal response of the sensor under constant and increasing pressure respectively, f) Sensitivity plot the fabricated sensor with a value of 14.959 kPa^{-1}, g) Stability of the fabricated sensor which displayed durability up to ~2500 cycles, h) Rise and fall time of ~99 msec and ~187 msec of the sensor at ~1.477 kPa of applied pressure.

Strain Sensing:

The digital image of the fabricated $Ti_3C_2T_x$ / $SnSe_2$ strain sensor with 3 cm x 2 cm dimensions was encapsulated in PDMS was employed for strain characterization is illustrated in figure 5a below. Figure 5b displays the I-V characteristics of the fabricated sensor in between -1V to 1V voltage range, which showed the increase in the value of the current response with a comparable increase in the value of the applied pressure. In figure 5c, it was observed that the sensor was capable of detecting the applied strain of ~15%, which describes the repeatability of the sensor response. The temporal response plots demonstrated in Figures 5d, and 5e substantiate that the upsurge in the current response was attained by increasing the external pressure applied and noticed that obtained results were consistent with the I-V characteristics of the fabricated sensor. In figure 5f, the gauge factor of the fabricated sensor displayed a value of 14.108 by plotting normalized resistance ($\Delta R/R_o\%$) against the applied strain ($\varepsilon\%$). Furthermore, figure 5g describes the durability of the fabricated sensor, which persists ~3000 cycles without an apparent change in the current response. Figure 5h denotes the response and recovery time of the sensor as ~296 msec and ~94 msec, respectively.

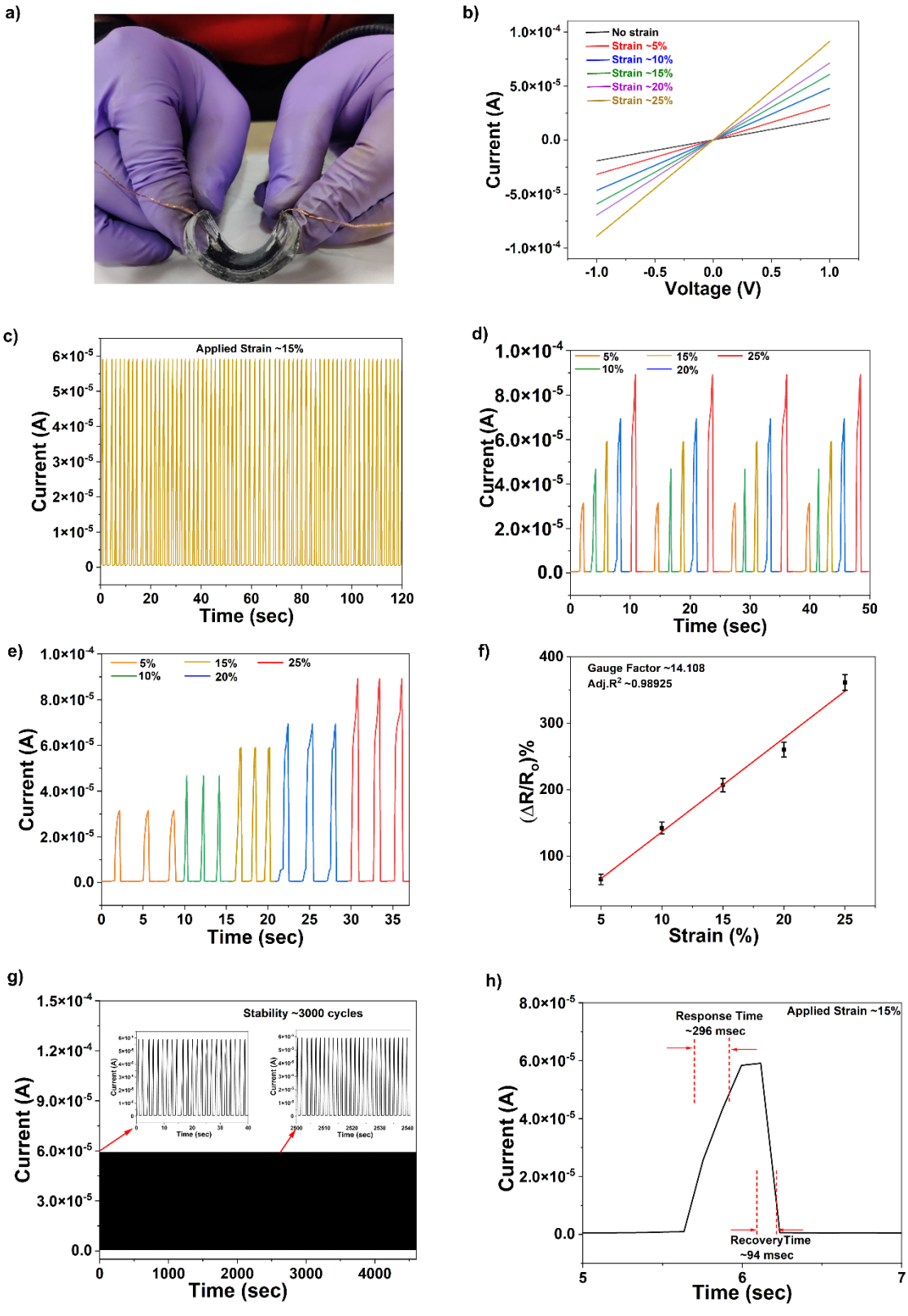
a)
b)
No strain
Strain ~5%
Strain ~10%
Strain ~15%
Strain ~20%
Strain ~25%
Current (A)
Voltage (V)
c)
Applied Strain ~15%
Current (A)
Time (sec)
d)
5%
10%
15%
20%
25%
Current (A)
Time (sec)
e)
5%
10%
15%
20%
25%
Current (A)
Time (sec)
f)
Gauge Factor ~14.108
Adj.R² ~0.98925
(ΔR/R₀)%
Strain (%)
g)
Stability ~3000 cycles
Current (A)
Time (sec)
h)
Response Time
~296 msec
Applied Strain ~15%
RecoveryTime
~94 msec
Current (A)
Time (sec)

Figure 5: Strain characterization of $Ti_3C_2T_x$ / $SnSe_2$ nanohybrid sensor a) Digital image of the fabricated sensor, b) I-V characteristics of the fabricated sensor, c),d),e) Temporal response of the sensor under constant and increasing strain respectively, f) Gauge Factor of the fabricated sensor was noted to be a value of 14.108, g) Stability of the fabricated sensor which displayed durability up to ~3000 cycles, h) Rise and fall time of ~296 msec and ~94 msec of the sensor at ~15% of applied strain.

Sensing Mechanism (Pressure and strain):

The synergistic behaviour of MXene / TMD nanohybrid leads to enhanced physical sensing performance which can primarily be stated due to a decrease in two types of resistances to the application of pressure and compressive bending strain viz. i) Tunnelling resistance, i.e. intrinsic piezoresistive property of the constituent layered materials (pressure effect) and overlapping of nanostructures to form conductive pathways (compressive strain effect); ii) Schottky barrier height (SBH) of the formed metal-semiconductor contacts, i.e. invariable lowering of the Schottky barrier with the application of pressure and overlaps leading to electron injection from semiconductor to metal thus increasing electron transport.

When pressure load is applied, the interlayer distance between the layered nanostructures of $Ti_3C_2T_x$ and $SnSe_2$ decreases and lowers than the tunnelling distance, resulting in increased plausibility of interlayer electron hopping, ultimately resulting in enhanced conductivity[7]. Likewise, with the application of compressive bending strain, i.e., when the sensor is bent inward, it leads to overlapping of $Ti_3C_2T_x$ layers and $SnSe_2$ nano balls like structure forming more conductive pathways resulting in a decrease in tunnelling resistance[8]. The following equation can quantitatively describe tunnelling resistance

$$R_{tunnel} = \frac{V}{aJ} = \frac{2}{3}\frac{h^2 t}{ae^2\sqrt{2m\phi}} exp(\frac{4\pi}{h}\sqrt{2m\phi t})$$

Notably, the tunnelling resistance is directly proportional to $te^{\sqrt{t}}$ which dictates that tunnelling resistance drops steeply with a decrease in thickness of void space (t), i.e. insulating medium between the layers and the overlapping region of nanostructures[9]. The corresponding figure 6illustrates a decrease in equivalent parallel resistance R_{SnSe2} and $R_{Ti3C2Tx}$ due to a reduction in tunnelling resistance of R_1 to R_n and R_1' to R_n' respectively, with the application of pressure. Further, in the case of compressive strain, the overlapping leads to a decrease in tunnelling distance, thus decreasing equivalent $R_{tunnel\ SnSe2}$ and $R_{tunnel\ Ti3C2Tx,}$ respectively.

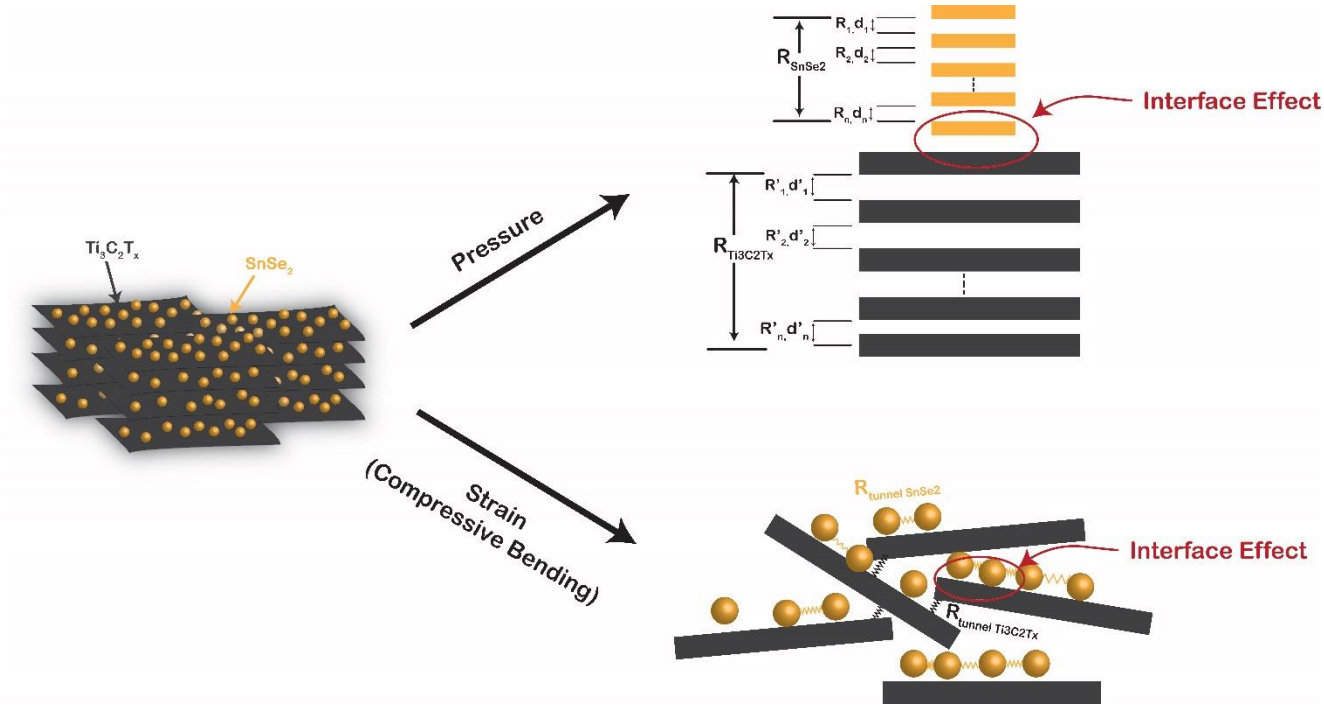

Figure 6: Schematic illustration for detailed sensing mechanism of the fabricated $Ti_3C_2T_x$ / $SnSe_2$ sensor

However, at the interface of metal-like $Ti_3C_2T_x$ and n-type semiconductor $SnSe_2$, a Schottky contact is formed, which governs the electron flow between both constituent active sensing materials. With the in-pot hydrothermal growth of $SnSe_2$ on $Ti_3C_2T_x$ coated cotton fabric, numerous heterojunctions are formed between the nanohybrid. To elucidate the interface phenomena on the sensing performance, qualitative band alignment before and after the contact formation is being sketched from the reported values for $Ti_3C_2T_x$ work function, electron affinity and bandgap of $SnSe_2$ in the literature[10,11] as shown in figure 7. Immediately after the contact formation, a potential barrier for flow of charge carrier is formed termed as Schottky barrier, and the barrier height can be defined using the ideal case Schottky-Mott model for an n-type semiconductor as:

$$\varphi_B = \varphi_{\mathrm{MXene}} - \chi_{SnSe2}$$

Where, φ_B is Schottky barrier height (SBH), φ_{MXene} is the work function of $Ti_3C_2T_x$ and χ_{SnSe2} is the electron affinity of n-type $SnSe_2$.

With the external stimuli of pressure or overlaps, the SBH (φ_B) invariably lowers at various heterojunctions to φ'_B which leads to the spontaneous injection of electrons from n-type semiconductor to metal, eventually resulting in the increased current response.

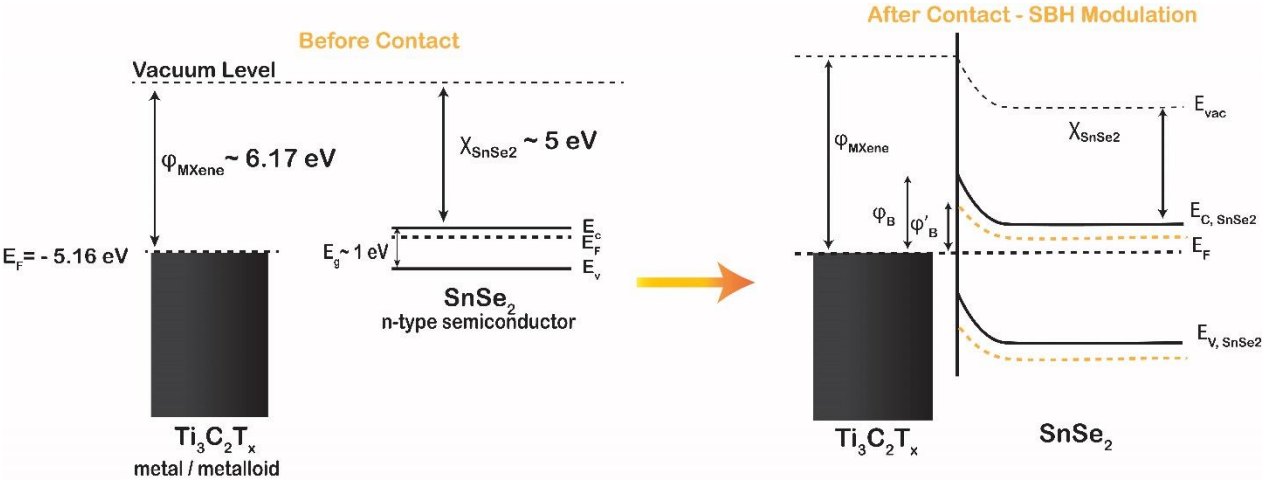

Figure 7: Illustration for the interface phenomena of the fabricated sensor before and after contact.

Temperature Sensing:

The fabricated $Ti_3C_2T_x$ / $SnSe_2$ was also utilized as a temperature sensor, wherein the fabricated device displayed in figure 8a was connected to the source meter and further placed in the closer proximity of the hot plate (~5mm distance) to note the temperature sensor readings. However, the resistance value of the fabricated sensor was observed to decrease by increasing the temperature on the hot plate from room temperature, i.e. 25 ^oC to 120 ^oC, exhibiting a negative temperature coefficient of resistance (TCR). In particular, to maintain the stabilized temperature, a break-off time of ~20 seconds was maintained for each successive measurement. The TCR value of the fabricated sensor was calculated to be 7.943 x 10^{-3} $^oC^{-1}$ obtained from the plot displayed in figure 8b, which is defined by $\alpha = 1/R_o \times (dR/dT)$, wherein R_o is the initial resistance of the fabricated sensor at room temperature. Also, the attained TCR value was more significant than the commercially existing platinum-based temperature sensors. However, the sensor will be more sensitive to the temperature variations when the TCR value is higher. The activation energy of the fabricated sensor was found to be 300.684 meV, which was obtained by plotting ln(R) against the inverse of temperature $(T^{-1})K^{-1}$ shown in figure 8c. The sensor will be more sensitive towards the temperature variations when the activation energy of the fabricated sensor is high and vice-versa.[12] The $Ti_3C_2T_x$ / $SnSe_2$ based nanohybrid device owing to excellent temperature sensing capabilities,

has found possible applications in the wearable electronics field to detect the temperature variations of the human body.

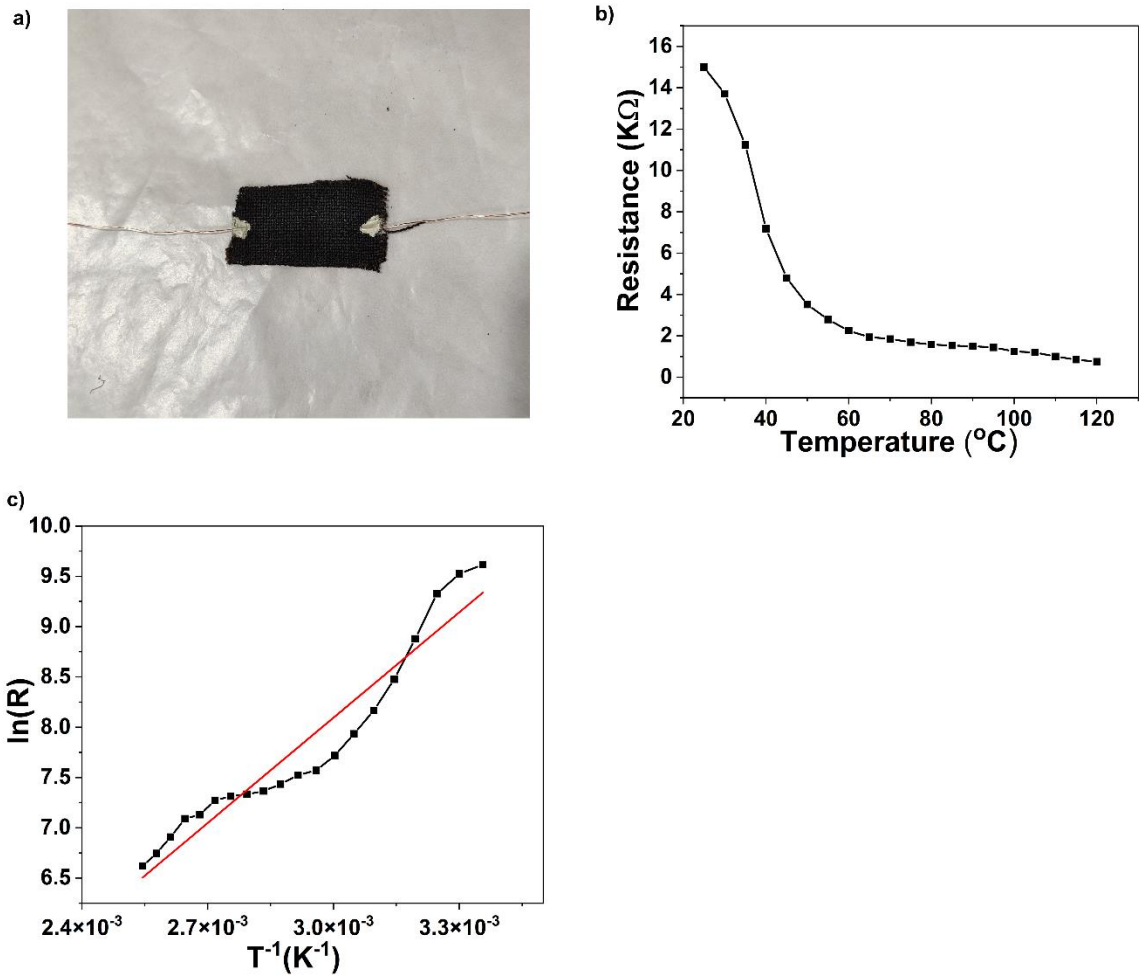

Figure 8: a) Digital image of the fabricated $Ti_3C_2T_x$ / $SnSe_2$ temperature sensor, b) Plot displaying resistance plotted against temperature, c) Arrhenius plot (i.e. ln(R) *vs* T^{-1})

Wireless integration of the fabricated sensors:

In the present study, the connections are established between the Raspberry Pi 3a controller and the analogue to digital converter, which in this case is an Adafruit MCP3008. Because the Raspberry Pi can only accept digital inputs through its general-purpose input-output ports, an analogue to digital converter is required to transform the analogue input acquired from the sensor to a digital value. The fabricated $Ti_3C_2T_x$ / $SnSe_2$ sensor is connected to any of the eight channels available in the MCP3008 ic. After the connections have been established, a code is run to detect the change in resistance as pressure, temperature, and strain are applied to the sensor. Because firebase is a free service with many analytical tools for remote monitoring, we used an external web-based API to create the database. The database saves and shows the incoming values from the Raspberry Pi as needed. These values are then transferred to an android/iOS/web-based app, which may be used to display and even plot the user's desired parameters. If internet connectivity is limited or absent, the android app may communicate with the raspberry pi over Bluetooth and obtain the same results. As a result, the entire system is constantly in sync and can be monitored remotely, which is an essential aspect of health care. The Schematic representation of wireless communication of the fabricated sensor is shown in figure 9. Also, the schematic layout for the fabricated sensor connected to the electronic circuit using various electronic components is shown below in figure 10a. The illustration for the interface between raspberry pi and MCP3008 IC configuration is displayed in figure 10b below

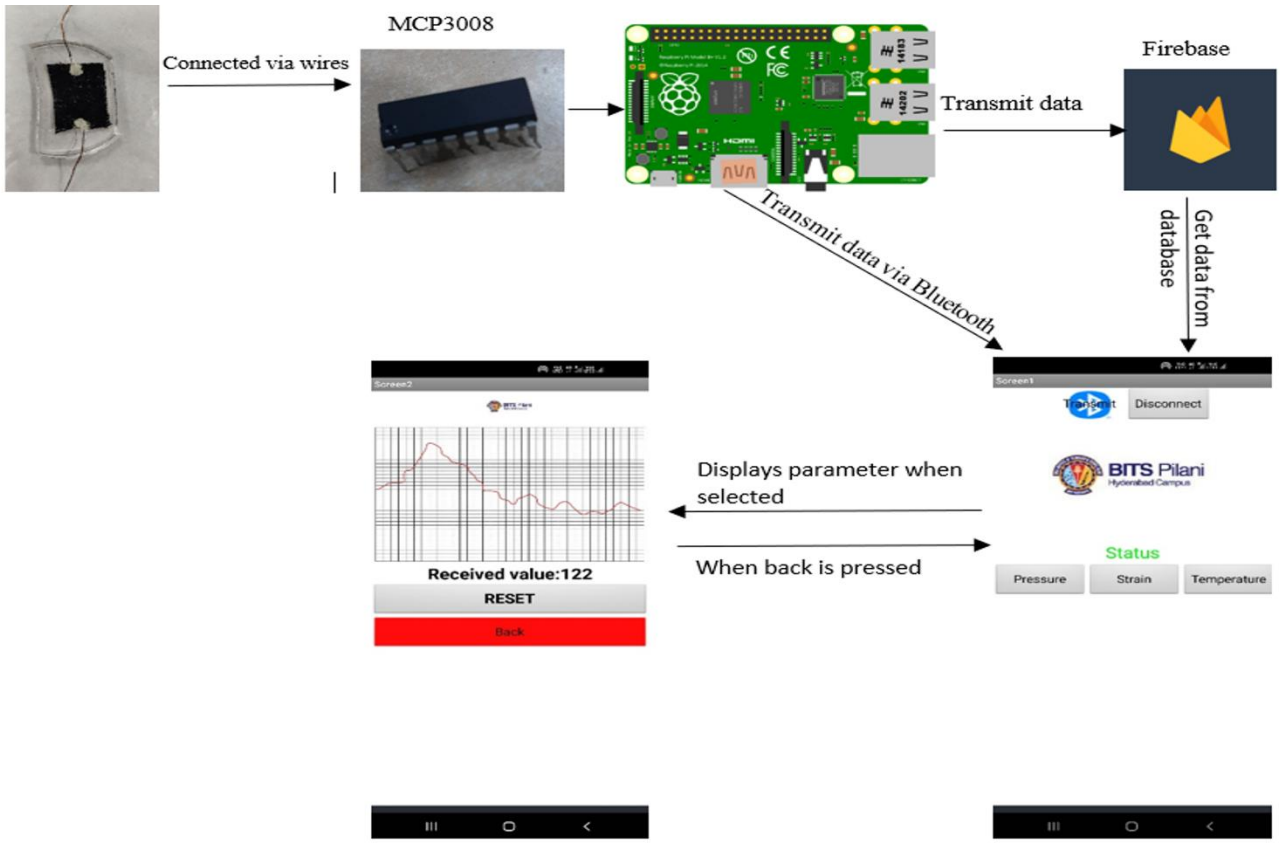

Figure9: Schematic representation of wireless communication of the fabricated sensor

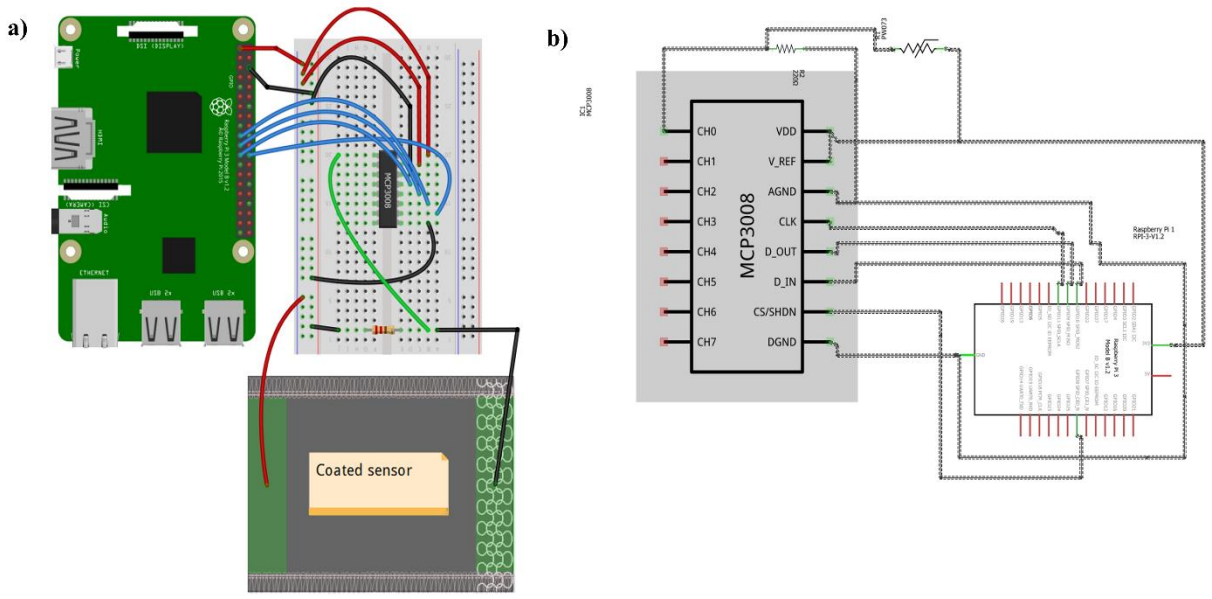

Figure10: a) Schematic layout for fabricated sensor connected to the electronic circuit using various electronic components, b) Schematic for the interface between raspberry pi and MCP3008 IC configuration

Applications:

Pressure Sensing Application:

(i) Wearable smart shoe:

The m-technology based wearable smart shoe system and the mixture of communications, detection, and human-machine interface-based technologies aim to therapy and examine patients for hastening detection of diseases. The critical aspect of the smart shoe is thorough observation for the unwell patient and to improve athletes performance via facilitating medical specialists in the diagnosis and assessment.[13] Herein, the $Ti_3C_2T_x$ / $SnSe_2$ sensor was integrated inside the shoe by attachment to socks and later used for continuous monitoring of running and walking patterns of an individual in place for 60 seconds is demonstrated in figure 11 below.

Owing to motion, landing and lifting off the feet, current response changes were observed. Further, the elevation in the frequency of sharp peaks signifies the running pattern of an individual. In addition, the fabricated sensor also finds potential applications to estimate the exact positioning of feet during human motion in daily life activities to avoid medical complexities.

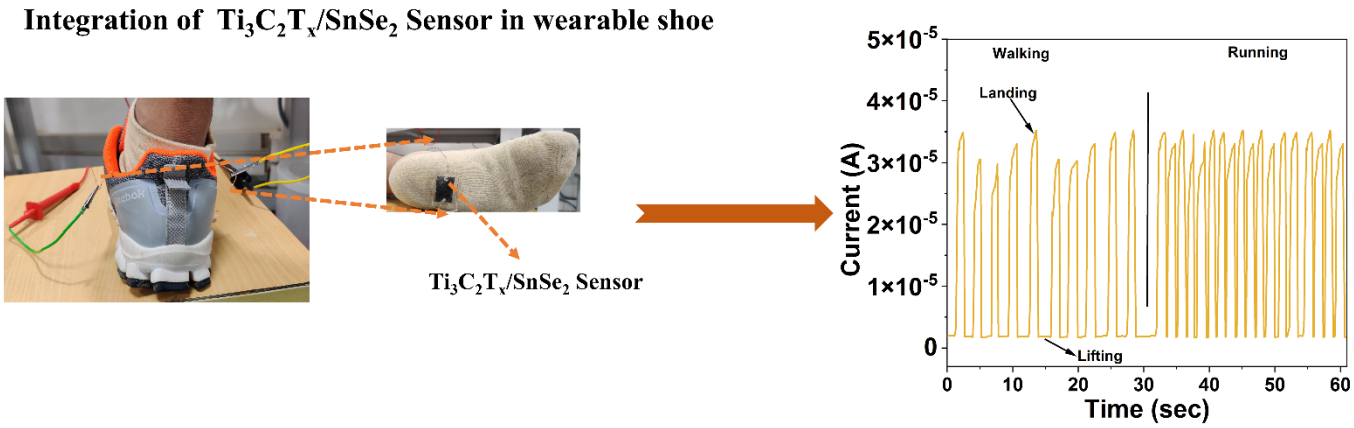

Figure 11: $Ti_3C_2T_x$ / $SnSe_2$ sensor-based smart shoe system used to sense walking and running patterns for 60 seconds.

Strain Sensing Application

(ii) Smart Crepe bandage:

The requirement for E-textile based extensively sensitive wearable sensors has been increased for examining health during life activities. Herein, the $Ti_3C_2T_x$ / $SnSe_2$ nanohybrid based E-textile sensor was integrated into the crepe bandage and noted the temporal response at various bending angles. Subsequently, an increase in the current response was observed by increasing the applied strain at varied bending angles, depicted in figure 12 below. In particular, in bending angles1, 2, and 3 shown in the insets of figure 12 has exhibited a current response of

~40 µA, ~70 µA and ~93 µA, respectively. Further, the fabricated E-textile-based smart crepe bandage has potential applications in smart medical textiles.

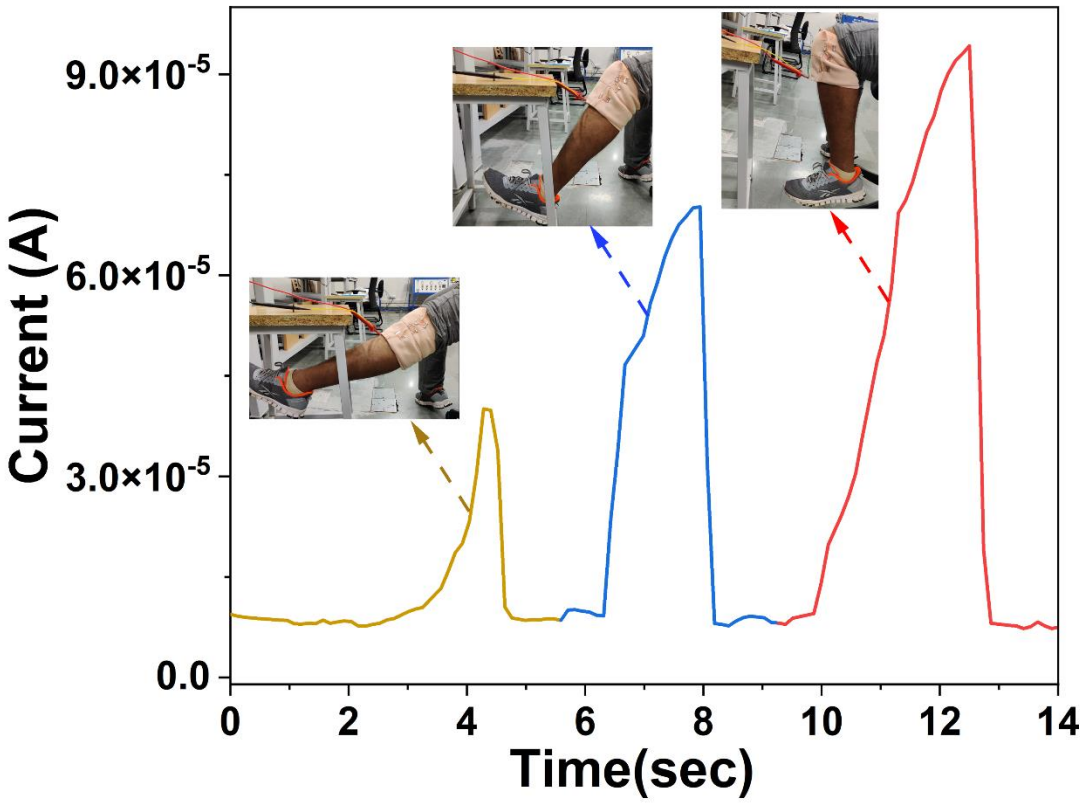

Figure12: Temporal response plot for $Ti_3C_2T_x$ / $SnSe_2$ nanohybrid based E-textile Smart Crepe bandage at varied bending angles

State of Art:

The performance comparison of $Ti_3C_2T_x$ / $SnSe_2$ based nanohybrid E-textile based physical sensors with other reported textile-based physical sensors is tabulated in Table 1 below. Shirley *et al.* fabricated ZnO nanostructure-based textile-based pressure sensor *via* hydrothermal route and attained a sensitivity value of 0.08 mV kPa^{-1}. Liu *et al.* fabricated a flexible graphene-silk fabric sensor by employing the dip-coating technique and obtained a sensitivity value of 0.4 kPa^{-1} for

applied 0-140 kPa pressure range. Wang *et al.* fabricated an MXene coated air-permeable pressure sensor on cotton fabric *via* the dip-coating method and displayed a sensitivity value of 7 kPa^{-1}. Zhou *et al.*fabricated a wearable high-performance $Ti_3C_2T_x$ based strain sensor using the dip-coating method and obtained a gauge factor of 4.11 at 3-15% of applied strain. Uzun *et al.* fabricated highly conductive MXene coated cellulose yarns and utilized them as a strain sensor which displayed a gauge factor of 6.02 up to 20% of applied strain. In the present work, $Ti_3C_2T_x$ / $SnSe_2$ nanohybrid-based piezoresistive sensor was fabricated using a hydrothermal/ dip-coating method and acquired sensitivity of 14.959 kPa^{-1} and a gauge factor of 14.108, respectively.

Table 1: Performance comparison of $Ti_3C_2T_x$ / $SnSe_2$ based nanohybrid physical sensor with reported literature

Material	**Substrate**	**Deposition Technique**	**Range of Detection**	**Pressure Sensitivity (kPa^{-1})**	**Gauge Factor**	**References**
ZnO	Conductive woven fabric	Hydrothermal	0-300 kPa	0.08 $x10^{-3}$	-	[14]
Graphene	Silk fabric	Dip-Coating	0-140 kPa	0.4	-	[15]
$Ti_3C_2T_x$	Cotton	Dip-coating	1-2	7.67	-	[16]
MXene	Cotton	Dip-coating	ε =3% - 15%	-	4.11	[17]

MXene	Knitted Cellulose Yarns	Dip-coating	ε =5% - 20%	-	6.02	[18]
$Ti_3C_2T_x$	Textile	Dip-Coating	29-40 kPa	12.095 at 29-40 kPa	-	[19]
$Ti_3C_2T_x$ / $SnSe_2$	**Cotton fabric**	**Dip-Coating and Hydrothermal**	**1.477 kPa – 3.456 kPa, ε =5%-25%**	**14.959 kPa^{-1} at 1.477 kPa – 3.185 kPa**	**14.108**	**This Work**

Conclusion:

In summary, we deposited $Ti_3C_2T_x$/ $SnSe_2$ thin-film on the cotton substrate *via a* cost-effective one-step hydrothermal approach followed by Dip coating technique and later fabricated multifunctional physical sensors (pressure, strain, and temperature) for non-invasive health care applications. The fabricated nanohybrid E-textile based physical sensors, i.e. pressure and strain, displayed an enhanced sensitivity of 14.959 kPa^{-1} for 1.477–3.456 kPa of the applied external pressure and an improved gauge factor of 14.108 for 5-25% of applied strain. Also, these physical sensors have shown exceptional stability of ~2500 cycles for a pressure sensor and ~3000 cycles for a strain sensor which signifies the sturdiness of the sensor. Furthermore, the fabricated temperature sensor has displayed a TCR value of 7.943 x 10^{-3} $^oC^{-1}$ and a high activation energy

value of 300.684 meV. Additionally, an android/iOS/web-based app was developed to validate wireless integration of the fabricated multifunctional physical sensors by utilizing a simple electronic circuit. The successful demonstration of $Ti_3C_2T_x$/ $SnSe_2$ nanohybrid E-textile based multifunctional physical sensor commences new possibilities for advanced health care and medical applications.

ACKNOWLEDGEMENT

PS acknowledges the funding from SERB (SRG/2020/000098). PS acknowledges Birla Institute of Technology and Science Pilani, Hyderabad Campus for ACRG funding. The authors thank Central Analytical Laboratory, BITS Pilani Hyderabad Campus, for the aid in material characterization.

Conflicts of Interest

The authors declare further no conflicts of interest.

References:

(1) Adepu, V.; Mattela, V.; Sahatiya, P. Remarkably Ultra-Sensitive Large Area Matrix of MXene Based Multifunctional Physical Sensors (Pressure, Strain, and Temperature) for Mimicking the Human Skin. *J. Mater. Chem. B* **2021**, *9* (22), 4523–4534.

(2) Halim, J.; Lukatskaya, M. R.; Cook, K. M.; Lu, J.; Smith, C. R.; Na, L.-åke; May, S. J.; Hultman, L.; Gogotsi, Y.; Eklund, P.; et al. Transparent Conductive Two-Dimensional Titanium Carbide Epitaxial Thin Films. *Chem. Mater.* **2014**, *26* (7), 2374–2381.

(3) Ghidiu, M.; Halim, J.; Kota, S.; Bish, D.; Gogotsi, Y.; Barsoum, M. W. Ion-Exchange and Cation Solvation Reactions in Ti3C2 MXene. *Chem. Mater.* **2016**, *28* (10), 3507–3514.

(4) Yang, H.; Liu, H.; Liu, X.; Zhao, Z.; Luo, J. Electroreduction of Carbon Dioxide to Formate over a Thin-Layered Tin Diselenide Electrode. *Catal. Sci. Technol.* **2018**, *8* (21), 5428–5433.

(5) Search, H.; Journals, C.; Contact, A.; Iopscience, M.; Phys, S. S.; Address, I. P. Raman Scattering Studies of SnS2 and SnSe2 (1997). *J. Phys. C Solid State Phys.* **1977**, *10* (8), 1321–1323.

(6) Hu, T.; Wang, J.; Zhang, H.; Li, Z.; Hu, M.; Wang, X. Vibrational Properties of Ti3C2 and Ti3C2T2 (T = O, F, OH) Monosheets by First-Principles Calculations: A Comparative Study. *Phys. Chem. Chem. Phys.* **2015**, *17* (15), 9997–10003.

(7) Ma, Y.; Liu, N.; Li, L.; Hu, X.; Zou, Z.; Wang, J.; Luo, S.; Gao, Y. A Highly Flexible and Sensitive Piezoresistive Sensor Based on MXene with Greatly Changed Interlayer Distances. *Nat. Commun.* **2017**, *8* (1), 1–7.

(8) Veeralingam, S.; Sahatiya, P.; Kadu, A.; Mattela, V.; Badhulika, S. Direct, One-Step Growth of NiSe2on Cellulose Paper: A Low-Cost, Flexible, and Wearable with Smartphone Enabled Multifunctional Sensing Platform for Customized Noninvasive Personal Healthcare Monitoring. *ACS Appl. Electron. Mater.* **2019**, *1* (4), 558–568.

(9) Wang, B.; Shi, T.; Zhang, Y.; Chen, C.; Li, Q.; Fan, Y. Lignin-Based Highly Sensitive Flexible Pressure Sensor for Wearable Electronics. *J. Mater. Chem. C* **2018**, *6* (24), 6423–6428.

(10) Zuo, G.; Wang, Y.; Teo, W. L.; Xie, A.; Guo, Y.; Dai, Y.; Zhou, W.; Jana, D.; Xian, Q.; Dong, W.; et al. Ultrathin ZnIn2S4 Nanosheets Anchored on Ti3C2TX MXene for Photocatalytic H2 Evolution. *Angew. Chemie - Int. Ed.* **2020**, *59* (28), 11287–11292.

(11) Guo, Y.; Robertson, J. Band Engineering in Transition Metal Dichalcogenides: Stacked versus Lateral Heterostructures. *Appl. Phys. Lett.* **2016**, *108* (23).

(12) Sahatiya, P.; Kadu, A.; Gupta, H.; Thanga Gomathi, P.; Badhulika, S. Flexible, Disposable Cellulose-Paper-Based MoS2/Cu2S Hybrid for Wireless Environmental Monitoring and Multifunctional Sensing of Chemical Stimuli. *ACS Appl. Mater. Interfaces* **2018**, *10* (10), 9048–9059.

(13) Saidani, S.; Haddad, R.; Mezghani, N.; Bouallegue, R. A Survey on Smart Shoe Insole Systems. In *2018 International Conference on Smart Applications, Communications and Networking, SmartNets 2018*; IEEE, 2018.

(14) Shirley, J. A.; Florence, S. E.; Sreeja, B. S.; Padmalaya, G.; Radha, S. Zinc Oxide Nanostructure-Based Textile Pressure Sensor for Wearable Applications. *J. Mater. Sci. Mater. Electron.* **2020**, *31* (19), 16519–16530.

(15) Liu, Y.; Tao, L. Q.; Wang, D. Y.; Zhang, T. Y.; Yang, Y.; Ren, T. L. Flexible, Highly Sensitive Pressure Sensor with a Wide Range Based on Graphene-Silk Network Structure. *Appl. Phys. Lett.* **2017**, *110* (12). https://doi.org/10.1063/1.4978374.

(16) Liu, R.; Li, J.; Li, M.; Zhang, Q.; Shi, G.; Li, Y.; Hou, C.; Wang, H. MXene-Coated Air-Permeable Pressure-Sensing Fabric for Smart Wear. *ACS Appl. Mater. Interfaces* **2020**, *12* (41), 46446–46454.

(17) Liu, L.; Wang, L.; Liu, X.; Yuan, W.; Yuan, M.; Xia, Q.; Hu, Q.; Zhou, A. High-Performancewearable Strain Sensor Based on Mxene@cotton Fabric with Network Structure. *Nanomaterials* **2021**, *11* (4), 889.

(18) Uzun, S.; Seyedin, S.; Stoltzfus, A. L.; Levitt, A. S.; Alhabeb, M.; Anayee, M.; Strobel, C. J.; Razal, J. M.; Dion, G.; Gogotsi, Y. Knittable and Washable Multifunctional MXene-Coated Cellulose Yarns. *Adv. Funct. Mater.* **2019**, *29* (45), 1–13.

(19) Li, T.; Chen, L.; Yang, X.; Chen, X.; Zhang, Z.; Zhao, T.; Li, X.; Zhang, J. A Flexible Pressure Sensor Based on an MXene-Textile Network Structure. *J. Mater. Chem. C* **2019**, *7* (4), 1022–1027.